



Velocity-induced numerical solutions of reaction-diffusion systems on continuously growing domains

Anotida Madzvamuse ^{a,*}, Philip K. Maini ^b

^a University of Sussex, Department of Mathematics, Mantell Building, Brighton, BN1 9RF England, UK

^b Centre for Mathematical Biology, Mathematical Institute, University of Oxford, 24–29 St Giles', Oxford OX1 3LB, UK

Received 24 March 2006; received in revised form 25 October 2006; accepted 16 November 2006

Available online 16 January 2007

Abstract

Reaction-diffusion systems have been widely studied in developmental biology, chemistry and more recently in financial mathematics. Most of these systems comprise nonlinear reaction terms which makes it difficult to find closed form solutions. It therefore becomes convenient to look for numerical solutions: finite difference, finite element, finite volume and spectral methods are typical examples of the numerical methods used. Most of these methods are locally based schemes. We examine the implications of mesh structure on numerically computed solutions of a well-studied reaction-diffusion model system on two-dimensional fixed and growing domains. The incorporation of domain growth creates an additional parameter – the grid-point velocity – and this greatly influences the selection of certain symmetric solutions for the ADI finite difference scheme when a uniform square mesh structure is used. Domain growth coupled with grid-point velocity on a uniform square mesh stabilises certain patterns which are however very sensitive to any kind of perturbation in mesh structure. We compare our results to those obtained by use of finite elements on unstructured triangular elements.

© 2006 Elsevier Inc. All rights reserved.

Keywords: Reaction-diffusion; Moving grid finite elements; ADI finite difference; Pattern formation; Schnakenberg model; Grid-point velocity; Growing domain

1. Introduction

In his seminal paper Turing [43] considered a system of two reacting and diffusing chemicals (which he termed morphogens) and demonstrated the surprising phenomenon of diffusion-driven instability. That is, he showed that it was possible for a spatially uniform steady state, linearly stable in the absence of diffusion, to be driven unstable by the presence of diffusion and evolve to a spatially non-uniform steady state. Reaction-diffusion models of this type have been studied in the context of pattern formation in hydra (Geirer and Meinhardt, [13]), sequential pattern formation in vertebrates (Meinhardt, [26]), animal coat markings (Murray, [31]), and shell pigmentation patterns (Meinhardt, [27]). Further examples can be found in Murray's book [32].

* Corresponding author. Tel.: +44 1273 87 3529.

E-mail address: a.madzvamuse@sussex.ac.uk (A. Madzvamuse).

Most of the above applications of Turing theory have assumed fixed domains. In the context of developmental biology, the tacit assumption is that the pattern forming processes occur on a different timescale to domain growth. However, it has been shown that in some cases this is not true and that domain growth can play a very important role in pattern formation and selection [17,9,34].

The rapid recent developments in computational power have given a new impetus to the application of novel numerical techniques to a wide variety of non-traditional mathematical fields. This is clearly observed in the life sciences, especially in mathematical biology and bio-medicine. With this comes the need to understand the basis of these numerical methods and the effects of mesh structure on numerical solutions. Most, if not all, numerical methods are based locally on mesh elements. For example, the centred finite difference scheme is based on a five-point stencil [29]. The finite element method [14] is element based, where the structure of the mesh could be as simple as segments, triangles, rectangles or as complex as tetrahedrons in one, two and three dimensions, respectively. These are not the only mesh-based numerical methods. The spectral method [5] and the finite volume scheme [29] are some of the numerical schemes which are mesh-dependent.

In this paper we concentrate on the most widely used finite difference and finite element methods. We are interested in numerical solutions of reaction-diffusion systems on fixed and continuously deforming domains. We investigate the role of mesh structure and regularity on the observed numerically computed solutions and illustrate our results by focusing on one particular well-known reaction-diffusion model.

The most widely used numerical method is the centred finite difference scheme mainly because it is computationally easy to implement and handles boundary conditions in a straightforward way. In most cases a regular uniform mesh is used on regular domains. For Turing reaction-diffusion models, illustrations of the use of such schemes to numerically compute solutions can be found in, for example, the papers by Murray [31], Kondo and Asai [17], Painter et al. [34], Barrio et al. [3,4], Crampin et al. [9] and more recently Plaza et al. [36].

On the other hand, the finite element method is more complicated to implement than the finite difference scheme. The basis of the finite element method involves a weak variational formulation of the partial differential equation system whereby the solution is sought in a finite-dimensional subspace. All computations are then restricted to local elements where local matrices are computed and then assembled into global matrices. The formulation is independent of the structure of the mesh although the mesh has to satisfy some criteria (see, for example, Reddy [37], Johnson [14], Morton [28] for specific details). Applications of finite elements to reaction-diffusion systems in developmental biology can be found, for example, in papers by Chaplain et al. [7], Sekimura et al. [40], Madzvamuse [25,19], Madzvamuse et al. [23,24,22,21,20], Nijhout et al. [33], Zheng et al. [44], and Cristini et al. [12].

The application of spectral methods to reaction-diffusion systems is not as widely used as the aforementioned methods. However, recently Kassam and Trefethen [15,16] have proposed a modified Exponential Time Differencing fourth-order Runge-Kutta (ETDRK4) method for solving stiff nonlinear partial differential equations of which reaction-diffusion systems are a particular case. The ETDRK4 scheme was found to be the best scheme for providing accurate stable solutions in a fast and efficient way on fixed domains. To our knowledge, this scheme has not been extended for application to spatially irregular complicated fixed, or sometimes growing domains. For further details on this method, see, for example, the papers by Kassam and Trefethen [15,16], Cox and Matthews [8], and Tadmor [42].

The aim of this paper is to illustrate through numerical solutions the role of mesh structure on solutions of reaction-diffusion equations on continuously deforming domains for the ADI finite difference scheme. It is known, though not well documented, that for nonlinear partial differential equations, the structure of the lattice (mesh elements) could greatly affect numerical solutions for finite difference schemes on fixed domains. We will illustrate computationally that domain growth coupled with grid-point velocity on a uniform square mesh stabilises certain patterns which are very sensitive to any kind of perturbation in mesh structure. The grid-point velocity and therefore the resolution of the computational domain plays an important role in the bifurcation process. The results of our numerical experiments will highlight the need to: (a) develop a bifurcation theoretical framework on continuously deforming domains and (b) carry out a detailed numerical analysis, for example, on artificial numerical diffusion which depends on the mesh structure and the domain growth. Both of these research threads are the focus of our current research studies.

This paper is organised as follows: in Section 2 we present the general reaction-diffusion model equations on a continuously deforming domain, and Section 3 deals with the numerical methods that we apply to solve these equations. Computational results illustrating the role of mesh structure are presented in Sections 4 and 5 on fixed and growing domains, respectively. Lastly we present our conclusions in Section 6.

2. Model equations

Consider the generalised nondimensional reaction-diffusion system of two chemical concentrations u and v on a continuously deforming domain (Crampin [10], Madzvamuse [25]):

$$u_t + \nabla \cdot (\mathbf{a}u) = \nabla^2 u + \gamma f(u, v), \quad (2.1)$$

$$v_t + \nabla \cdot (\mathbf{a}v) = d\nabla^2 v + \gamma g(u, v) \quad \text{in } \Omega(t), \quad (2.2)$$

with $\Omega(t)$ representing a time-dependent domain. Here \mathbf{a} represents the field flow velocity. $f(u, v)$ and $g(u, v)$ represent reaction kinetics, d is a constant ratio of the diffusion coefficients and γ is a scaling parameter. Initial conditions are prescribed as small random perturbations around the uniform steady state if it exists. Boundary conditions can either be periodic, zero-flux (homogeneous Neumann) or mixed. Zero-flux boundary conditions are appropriate for the case of an impermeable membrane, for example, or where we wish to explore self-organising processes. Periodic boundary conditions can represent, for example, the case of a closed, cylindrical domain.

Most studies of reaction-diffusion equations assume fixed regular domains. To consider a time-dependent domain, it is logical to try to transform the model equations (2.1) and (2.2) from a continuously deforming domain to a fixed domain where appropriate numerical schemes have already been developed and tested. One possible way to do this is to use Lagrangian transformations (Baines, [1]). This type of simplification yields partial differential equations with time-dependent coefficients on a fixed domain. The continuously deforming domain is transformed at each time to a fixed domain. Below we illustrate how this can be achieved.

2.1. Lagrangian transformations

In this section we look at the partial differential equations on continuously deforming domains from a Lagrangian point of view (see, for example, Baines, [1]). A transformation between a moving grid to a fixed grid is sought. Let ξ and η be fixed cartesian coordinates such that

$$x = \hat{x}(\xi, \eta, \tau), \quad y = \hat{y}(\xi, \eta, \tau) \quad \text{and} \quad t = \tau.$$

As t varies, the coordinates x and y change position with time. These positions are then mapped or transformed to a fixed position given by the ξ and η coordinates. Now under this transformation, suppose u is mapped into the new function defined as $u(x, y, t) = \hat{u}(\xi, \eta, \tau)$. We can compute the time-derivative using the principle of differentiation “following the motion”

$$\hat{u}_\tau = u_t + u_x \hat{x}_\tau + u_y \hat{y}_\tau = u_t + \mathbf{a} \nabla u, \quad (2.3)$$

where

$$u_x = \hat{u}_\xi \xi_x + \hat{u}_\eta \eta_x, \quad u_y = \hat{u}_\xi \xi_y + \hat{u}_\eta \eta_y \quad \text{and} \quad \mathbf{a} = (\hat{x}_\tau, \hat{y}_\tau)^T. \quad (2.4)$$

From these equations we can derive the second partial derivatives

$$u_{xx} = \hat{u}_{\xi\xi} \xi_x^2 + \hat{u}_{\xi\xi} \xi_{xx} + \hat{u}_{\eta\eta} \eta_x^2 + \hat{u}_{\eta\eta} \eta_{xx}, \quad (2.5)$$

$$u_{yy} = \hat{u}_{\xi\xi} \xi_y^2 + \hat{u}_{\xi\xi} \xi_{yy} + \hat{u}_{\eta\eta} \eta_y^2 + \hat{u}_{\eta\eta} \eta_{yy}. \quad (2.6)$$

Hence the equation for u can be written as follows:

$$\hat{u}_\tau - \mathbf{a} \cdot \nabla u + \mathbf{a} \cdot \nabla u + (\nabla \cdot \mathbf{a}) \hat{u} = \hat{u}_{\xi\xi} (\xi_x^2 + \xi_y^2) + \hat{u}_\xi (\xi_{xx} + \xi_{yy}) + \hat{u}_{\eta\eta} (\eta_x^2 + \eta_y^2) + \hat{u}_\eta (\eta_{xx} + \eta_{yy}) + \gamma f(\hat{u}, \hat{v})$$

That is

$$\hat{u}_\tau = \hat{u}_{\xi\xi}(\xi_x^2 + \xi_y^2) + \hat{u}_\xi(\xi_{xx} + \xi_{yy})t + \hat{u}_{\eta\eta}(\eta_x^2 + \eta_y^2) + \hat{u}_\eta(\eta_{xx} + \eta_{yy}) + \gamma f(\hat{u}, \hat{v}) - (\nabla \cdot \mathbf{a})\hat{u}. \quad (2.7)$$

Similarly for v we have

$$\hat{v}_\tau = d(\hat{v}_{\xi\xi}(\xi_x^2 + \xi_y^2) + \hat{v}_\xi(\xi_{xx} + \xi_{yy}) + \hat{v}_{\eta\eta}(\eta_x^2 + \eta_y^2) + \hat{v}_\eta(\eta_{xx} + \eta_{yy})) + \gamma g(\hat{u}, \hat{v}) - (\nabla \cdot \mathbf{a})\hat{v}. \quad (2.8)$$

For example, in one dimension the above equations reduce to

$$\hat{u}_\tau = \hat{u}_{\xi\xi}\xi_x^2 + \hat{u}_\xi\xi_{xx} + \gamma f(\hat{u}, \hat{v}) - (\nabla \cdot \mathbf{a})\hat{u}, \quad (2.9)$$

$$\hat{v}_\tau = d(\hat{v}_{\xi\xi}\xi_x^2 + \hat{v}_\xi\xi_{xx}) + \gamma g(\hat{u}, \hat{v}) - (\nabla \cdot \mathbf{a})\hat{v}. \quad (2.10)$$

Although we have managed to transform the original partial differential equations into (2.7) and (2.8) respectively, these are still very difficult to solve in general for arbitrary domain growth. One possible form of simplification is to consider that domain growth is uniform and isotropic. By isotropic we mean that the boundary curve deforms continuously at the same rate in all directions at all times. Let us consider the one-dimensional case and assume that domain growth is uniform and isotropic defined as follows:

$$\hat{x} = \rho(t)X_0(\xi), \quad \xi \in [0, 1]. \quad (2.11)$$

The function $\rho(t)$ represents how the domain grows. Computing the derivatives we have

$$\hat{x}_\xi = \rho(t)\frac{dX_0}{d\xi}, \quad \frac{dX_0}{d\xi} = 1 \Rightarrow \xi_{\hat{x}} = \frac{1}{\rho(t)}, \quad (2.12)$$

$$\hat{x}_{\xi\xi} = \rho(t)\frac{d^2X_0}{d\xi^2}, \quad \frac{d^2X_0}{d\xi^2} = 0. \quad (2.13)$$

Also

$$\hat{x}_\tau = \frac{d\rho}{dt}X_0(\xi) = \frac{d\rho}{dt}\xi = \frac{\dot{\rho}(t)}{\rho(t)}\hat{x}. \quad (2.14)$$

Therefore we can compute

$$\nabla \cdot \mathbf{a} = \frac{\dot{\rho}(t)}{\rho(t)}. \quad (2.15)$$

Finally Eqs. (2.9) and (2.10) simplify to

$$\hat{u}_\tau = \frac{1}{\rho(t)^2}\hat{u}_{\xi\xi} - \frac{\dot{\rho}(t)}{\rho(t)}\hat{u} + \gamma f(\hat{u}, \hat{v}), \quad (2.16)$$

$$\hat{v}_\tau = \frac{d}{\rho(t)^2}\hat{v}_{\xi\xi} - \frac{\dot{\rho}(t)}{\rho(t)}\hat{v} + \gamma g(\hat{u}, \hat{v}), \quad (2.17)$$

where $0 \leq \xi \leq 1$. Similarly, the two-dimensional equations on a planar domain can be simplified by considering an isotropic growth of the form

$$\hat{x}(\xi, \eta, t) = \rho(t)X_0(\xi, \eta) = \rho(t)\xi, \quad (2.18)$$

$$\hat{y}(\xi, \eta, t) = \rho(t)Y_0(\xi, \eta) = \rho(t)\eta, \quad (2.19)$$

where $\xi, \eta \in [0, 1] \times [0, 1]$. Clearly

$$\hat{x}_\xi = \rho(t), \hat{x}_\eta = 0, \hat{y}_\xi = 0, \hat{y}_\eta = \rho(t), \quad (2.20)$$

$$\hat{x}_{\xi\xi} = \hat{x}_{\eta\eta} = \hat{y}_{\xi\xi} = \hat{y}_{\eta\eta} = 0. \quad (2.21)$$

Hence the two-dimensional equations are given by

$$\hat{u}_\tau = \frac{1}{\rho(t)^2}\nabla^2\hat{u} - \frac{2\dot{\rho}(t)}{\rho(t)}\hat{u} + \gamma f(\hat{u}, \hat{v}), \quad (2.22)$$

$$\hat{v}_\tau = \frac{d}{\rho(t)^2}\nabla^2\hat{v} - \frac{2\dot{\rho}(t)}{\rho(t)}\hat{v} + \gamma g(\hat{u}, \hat{v}). \quad (2.23)$$

Observe that

$$\frac{d\hat{x}}{d\tau} = \dot{\rho}(t)\xi = \frac{\dot{\rho}(t)}{\rho(t)}\hat{x} \quad \text{and} \quad \frac{d\hat{y}}{d\tau} = \dot{\rho}(t)\eta = \frac{\dot{\rho}(t)}{\rho(t)}\hat{y}.$$

Therefore

$$\nabla \cdot \mathbf{a} = \frac{2\dot{\rho}(t)}{\rho(t)}. \quad (2.24)$$

Transforming the original PDEs from a continuously growing domain to a fixed domain using Lagrangian transformations results in the elimination of the convective terms.

For illustrative and comparison purposes we consider only the Schnakenberg [41] reaction kinetics (these have been well-studied – see for example [32])

$$f(u, v) = a - u + u^2v, \quad (2.25)$$

$$g(u, v) = b - u^2v. \quad (2.26)$$

Here a and b are constant (positive) parameters. Eqs. (2.1) and (2.2) are derived on an arbitrary continuously growing domain. Pattern selection does not only depend on the growth of the domain but also on its shape, for example, and the selection process can be curvature dependent. Plaza et al. [36] derived reaction-diffusion systems on a parametrized growing domain. Their equations included the rate of domain growth together with definitions of the curved boundaries. Eqs. (2.16), (2.17), (2.22) and (2.23) are particular cases of their generalised model equations. These equations were also derived independently by Crampin et al. [9].

3. Numerical methods

3.1. Alternating-direction implicit scheme

An Alternating-Direction Implicit (ADI) finite difference scheme is applied to solve the transformed system of equations (2.22) and (2.23) on a fixed domain at each time step. This scheme was first proposed by Peaceman and Rachford to model oil reservoirs [29]. The ADI is often thought of as an iterative linear solver for the five-point finite difference stencils on a rectangular grid (this is the original meaning used in the early papers by Peaceman and Rachford [35] for example). On the other hand, if iterated to convergence it merely becomes a split-step difference scheme and this is how we apply it in this paper. The ADI is characterized as follows: the integration is explicit in one direction and implicit in the other direction for one half-timestep, and the order is reversed for the other half-timestep. Details of how the ADI scheme is applied to reaction-diffusion systems can be found in papers by Crampin [10], Crampin et al. [9,11] and Painter et al. [34]. The ADI scheme is unconditionally stable, however in order to satisfy the conditions for the maximum principle the following bound needs to be met:

$$\max \left\{ \frac{\Delta t}{(\Delta x)^2}, \frac{\Delta t}{(\Delta y)^2} \right\} \leqslant 1.$$

The advantage of this scheme is that it gives rise to a tridiagonal form of the matrices. The tridiagonal system of equations can be solved fast and efficiently by using the Thomas algorithm [29]. The scheme is second order accurate in both time and space.

3.2. Moving grid finite element method

Unlike the finite difference scheme which is applied to the transformed equations, the moving grid finite element method is applied to the original equations (2.1) and (2.2) on a continuously deforming domain $\Omega(t)$. The method solves the model equations by use of piece-wise linear bases functions on an arbitrary continuously deforming domain. Here, an unstructured triangular mesh is used in the moving grid finite element simulations. The mesh is generated by a delaunay mesh generator package (Müller et al. [30]). The spatial discretization gives rise to a semi-discrete system of nonlinear ordinary differential equations. We use a second

order semi-implicit backward differentiation formula to discretise the ordinary differential equations in time. We shall abbreviate this method: the MGFEM-2SBDF scheme, to reflect the fact that we use moving grid finite elements in space and a second order semi-implicit backward differentiation formula in time. Details on implementation, stability and accuracy of the method can be found in the following papers: Madzvamuse [25,19], and Madzvamuse et al. [22,20]. The spatial discretisation gives rise to large sparse, symmetric and positive definite systems which are solved efficiently by using the preconditioned Conjugate Gradient method (Saad [39]).

It must be noted that it is also possible to use the transformed systems of equations (2.7)–(2.10) coupled with a time-dependent moving mesh equation which makes it possible to consider a more complicated domain growth (Cao et al. [6]).

4. Numerical experiments on two-dimensional fixed domains

This section aims to illustrate the point that the ADI and MGFEM-2SBDF schemes yield similar results in the absence of domain growth for zero-flux and periodic boundary conditions. In particular, we will highlight that for the ADI scheme the structure of the mesh can influence the selection of the numerical solution. In all our solutions we only show results corresponding to chemical concentration u , those of v are 180° out of phase to those of u . The colouration (shading) in figures for the ADI scheme is automatically generated in MatLab while those for the MGFEM scheme shading is done per triangular element. For further details see Madzvamuse et al. [25].

Let us take $\rho(t) = 1$ in equations (2.22) and (2.23) implying no domain growth. The reaction-diffusion equations (2.1) and (2.2) with Schnakenberg reaction kinetics reduce to the standard system

$$u_t = \nabla^2 u + \gamma(a - u + u^2 v), \quad (4.1)$$

$$v_t = d\nabla^2 v + \gamma(b - u^2 v), \quad (4.2)$$

on a fixed domain Ω .

4.1. Numerical experiment 1: Zero-flux boundary conditions

We compute numerical solutions to the model equations (4.1) and (4.2) on a unit square domain $[0, 1] \times [0, 1]$ with model parameter values $a = 0.1$, $b = 0.9$, $d = 10$ and (a) $\gamma = 114$, (b) $\gamma = 1000$, (c) $\gamma = 5000$. Let the timestep be taken as $\Delta t = 10^{-2}$ and compute solutions to final time, say, $t_F = 5$. Initial conditions are taken as small random perturbations around the homogeneous steady state $(1.0, 0.9)$ and zero-flux boundary conditions are applied.

The ADI scheme solves the model equations on a uniform mesh grid given by $\Delta x = \Delta y = \frac{1}{150}$ (Figs. 1 and 2). The MGFEM-2SBDF scheme solves the model equations on an unstructured triangular mesh of approximately 2000 nodes and 4000 elements. Fig. 1 illustrates solutions corresponding to the ADI scheme (left), and the MGFEM-2SBDF scheme (right). The values of γ are 114, 1000 and 5000 for the first, second and third rows respectively. The two schemes produce qualitatively similar solutions on fixed domains with zero-flux boundary conditions. We have shown in previous studies that the results obtained using the MGFEM scheme are independent of the structure of the mesh, regular, irregular or well-refined meshes yield similar results (Madzvamuse et al. [19–22]). Therefore the number of degrees of freedom quoted above for this scheme are simply for illustrative purposes.

4.2. Numerical experiment 2: Periodic boundary conditions

Following Ruuth [38] let the model parameter values be given by $a = 0.126779$, $b = 0.792366$, $d = 10.0$ and vary γ as before. We compute solutions on a fixed unit square domain with periodic boundary conditions

$$u(x = 0, y, t) = u(x = 1, y, t), \quad \text{and} \quad u(x, y = 0, t) = u(x, y = 1, t), \quad (4.3)$$

$$v(x = 0, y, t) = v(x = 1, y, t), \quad \text{and} \quad v(x, y = 0, t) = v(x, y = 1, t). \quad (4.4)$$

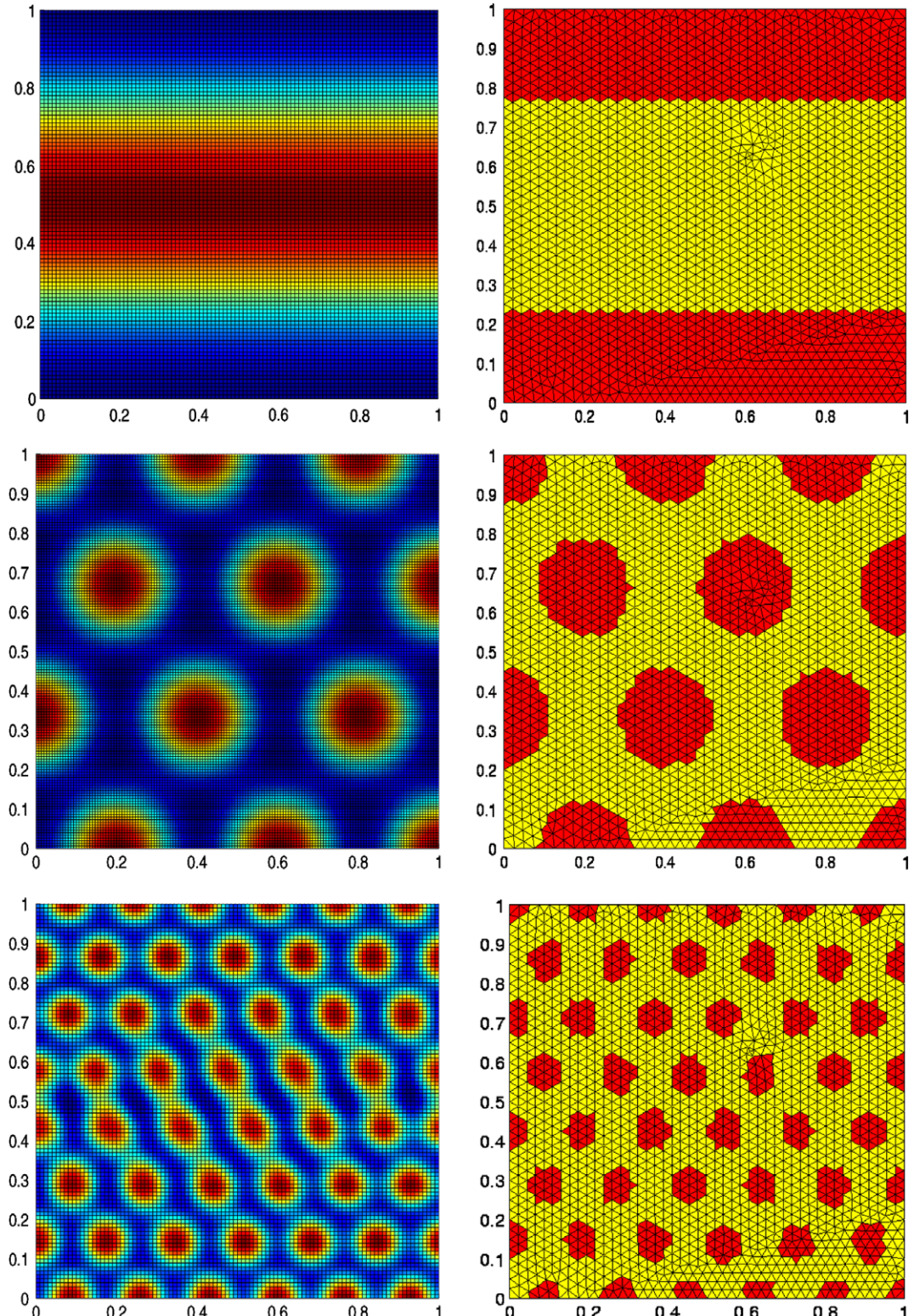


Fig. 1. The ADI (left column) and MGFEM-2SBDF (right column) steady state computational results for the u concentration of the model equations solved with zero-flux boundary conditions corresponding to parameter values $a = 0.1$, $b = 0.9$, $d = 10$ with $\gamma = 114$ (first row), $\gamma = 1000$ (second row) and $\gamma = 5000$ (third row).

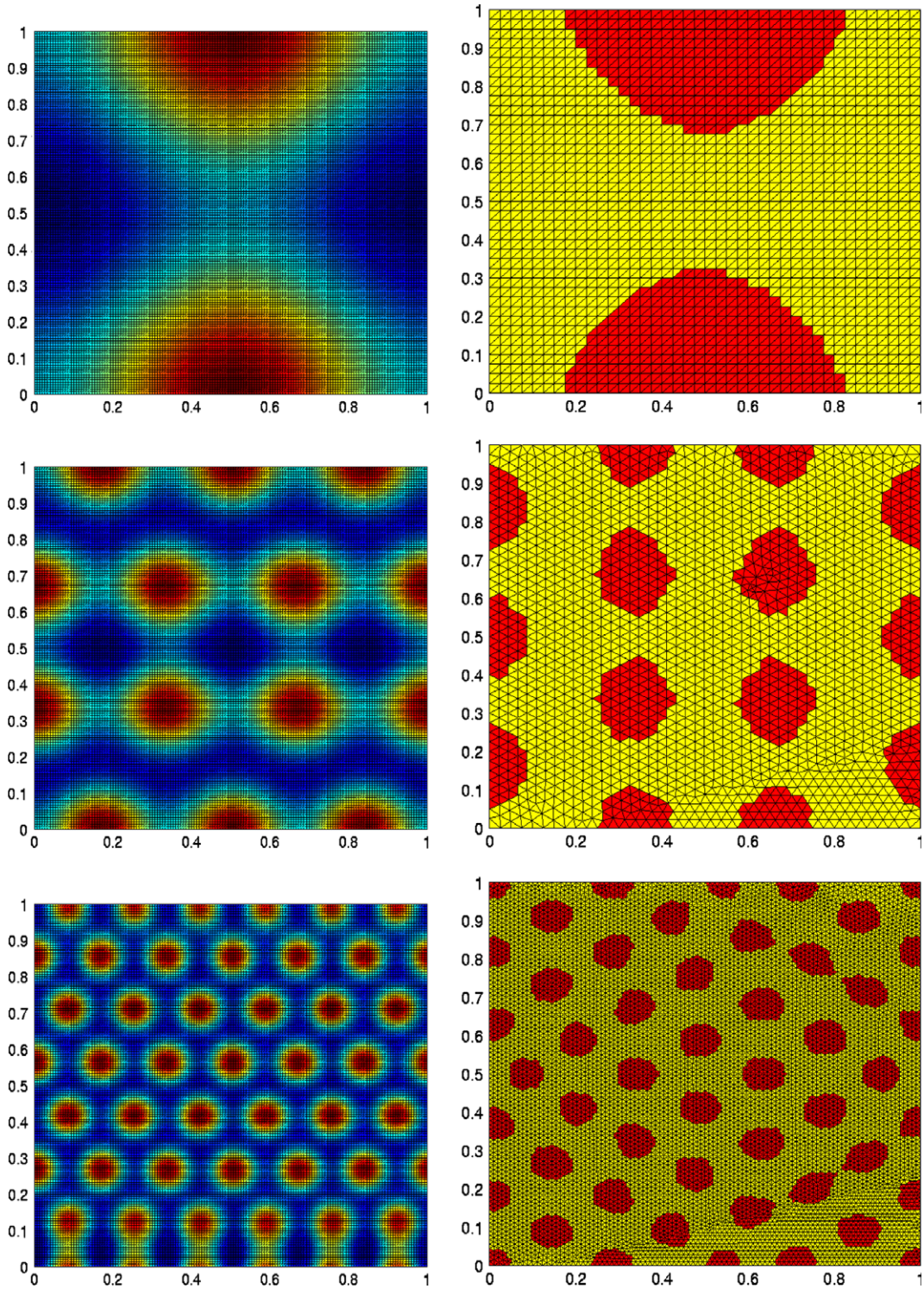


Fig. 2. The ADI (left) and MGFEM-2SBDF (right) steady state computational results for the u concentration of the model equations solved with periodic boundary conditions corresponding to parameter values $a = 0.126779$, $b = 0.792366$, $d = 10.0$ with $\gamma = 114$ (first row), $\gamma = 1000$ (middle row) and $\gamma = 5000$ (last row), respectively.

Initial conditions are prescribed as

$$u(\mathbf{x}, 0) = 0.919145 + 0.0016 \cos(2\pi(x+y)) + 0.01 \sum_{j=1}^8 \cos(2\pi jx), \quad (4.5)$$

$$v(\mathbf{x}, 0) = 0.937903 + 0.0016 \cos(2\pi(x+y)) + 0.01 \sum_{j=1}^8 \cos(2\pi jx). \quad (4.6)$$

Numerical solutions to the model equations are computed to some final time $t_F = 3$, say, with time-step $\Delta t = 10^{-5}$. As in experiment 1, we compute solutions using the ADI and MGFEM-2SBDF schemes and compare results. The results of these simulations are shown in Fig. 2. We draw attention to the second row for $\gamma = 1000$. The solution from the MGFEM-2SBDF scheme is a 90-degree rotation to that obtained from the ADI scheme. This is because of the symmetry of the square domain. For the ADI scheme, this is not the only final pattern observed. If we change the mesh structure from a uniform square mesh to a uniform rectangular mesh we obtain different results as illustrated in Figs. 3 and 4. In Fig. 3 we compute solutions to the model equations using the ADI scheme and illustrate the evolution of the approximate numerical solutions starting with stripe-like initial conditions for various mesh sizes. Numerical and parameter values as in Fig. 2 and the computations are carried out to final time $t_F = 1.0$. It can be observed that changing the mesh structure gives rise to different pattern generation sequences. This fact is demonstrated clearly in Fig. 4. Here we are only plotting the transient (left column) and steady state patterns (right column) for different mesh structure at time $t = 1.9$ and $t = 2.0$ respectively. From numerous computational experiments, the plots on the left column (top and bottom) are transient solutions just before they converge asymptotically to the steady states. The transient solutions evolve with time to either the top-right or the bottom-right inhomogeneous steady state pattern.

Imagine that we fold the square domains on the right column in Fig. 4 around the x -axis to form a cylinder with centre along the x -axis then the seemingly different patterns are identical. Although it seems that different mesh sizes give rise to different patterns, these in reality are identical solutions given periodic boundary conditions. Small changes in mesh size introduce noise into the numerical simulations which in turn influence the selection of the final pattern. Therefore the ADI and the MGFEM-2SBDF schemes provide qualitatively similar results in the absence of domain growth. The fact that for the ADI scheme, changes in the mesh structure from a uniform square mesh to a uniform rectangular mesh results in different transient solutions, on continuously deforming domains such changes influence dramatically the bifurcation process of the transient solutions as illustrated in the next section.

5. The role of mesh structure in numerical solutions for reaction-diffusion systems on growing domains

The aim of this section is to show through numerical simulations that for the ADI scheme changes in the mesh structure influence dramatically the bifurcation process of patterns on growing domains due to the grid-point velocity of the mesh and the resolution of the computational continuously deforming domain. Unlike the ADI scheme, the MGFEM-2SBDF scheme does not suffer from such bias due to the nature of its finite element formulation which is independent of the mesh structure.

Let us consider a continuously deforming unit square domain $[0, 1] \times [0, 1]$. Assume that domain growth is uniform and isotropic. Also assume that the domain grows exponentially with growth rate function defined by $\rho(t) = e^{rt}$ where $r = 0.002$ is the growth rate (Crankin, et al., [10,9]). All our simulations on growing domains are computed with the following model parameter values: $a = 0.1$, $b = 0.9$, $\gamma = 1.0$, $d = 0.01$. Zero-flux boundary conditions are imposed and initial conditions are prescribed as small random perturbations around the uniform steady state $(1.0, 0.9)$ obtained on a fixed domain. Transient solutions are computed to final time $t_F = 850.0$, i.e. the unit square domain is allowed to grow to approximately a 5.5×5.5 square domain. In order to compare with previous results in the literature, the ADI scheme solves the transformed system of equations (2.16)–(2.23) while the MGFEM scheme solves the non-transformed system of equations (2.1) and (2.2). We have shown in previous studies that the MGFEM method can be easily extended to more complicated irregular continuously deforming domains whose domain growth is prescribed through a specific definition or defined from experiments (Madzvamuse et al. [19–22]). This is contrary to the ADI scheme.

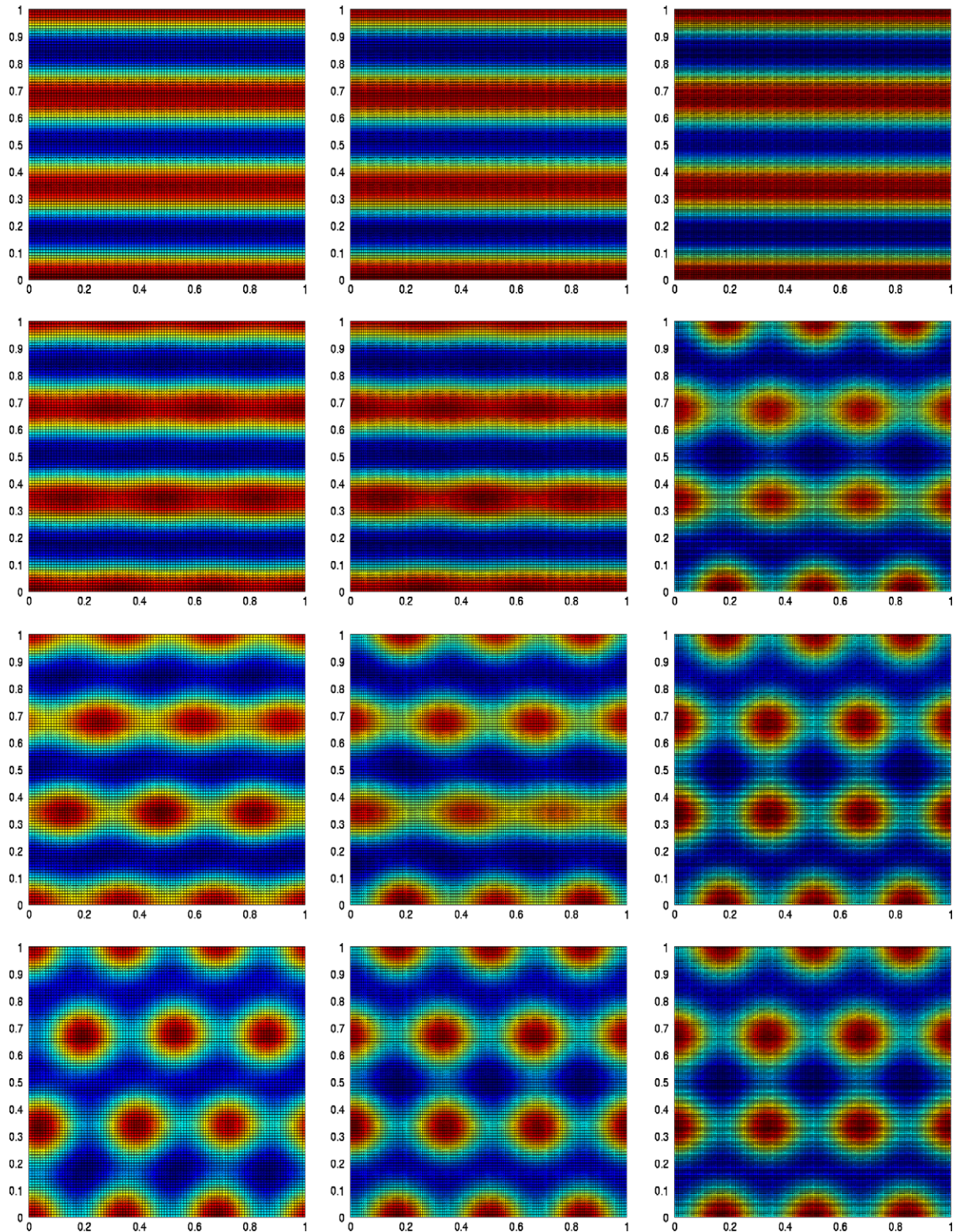


Fig. 3. Numerical solutions to the model equations solved by use of the ADI method with periodic boundary conditions at times $t = 0.042$ (first row), $t = 0.05$, (second), $t = 0.06$ (third) and $t = 1.0$ (fourth) respectively. Left: $\Delta x = \Delta y = \frac{1}{100}$, middle: $\Delta x = \frac{1}{150}$, $\Delta y = \frac{1}{100}$, and right: $\Delta x = \Delta y = \frac{1}{150}$. The parameter values are $a = 0.126779$, $b = 0.792366$, $d = 10.0$ and $\gamma = 1000$.

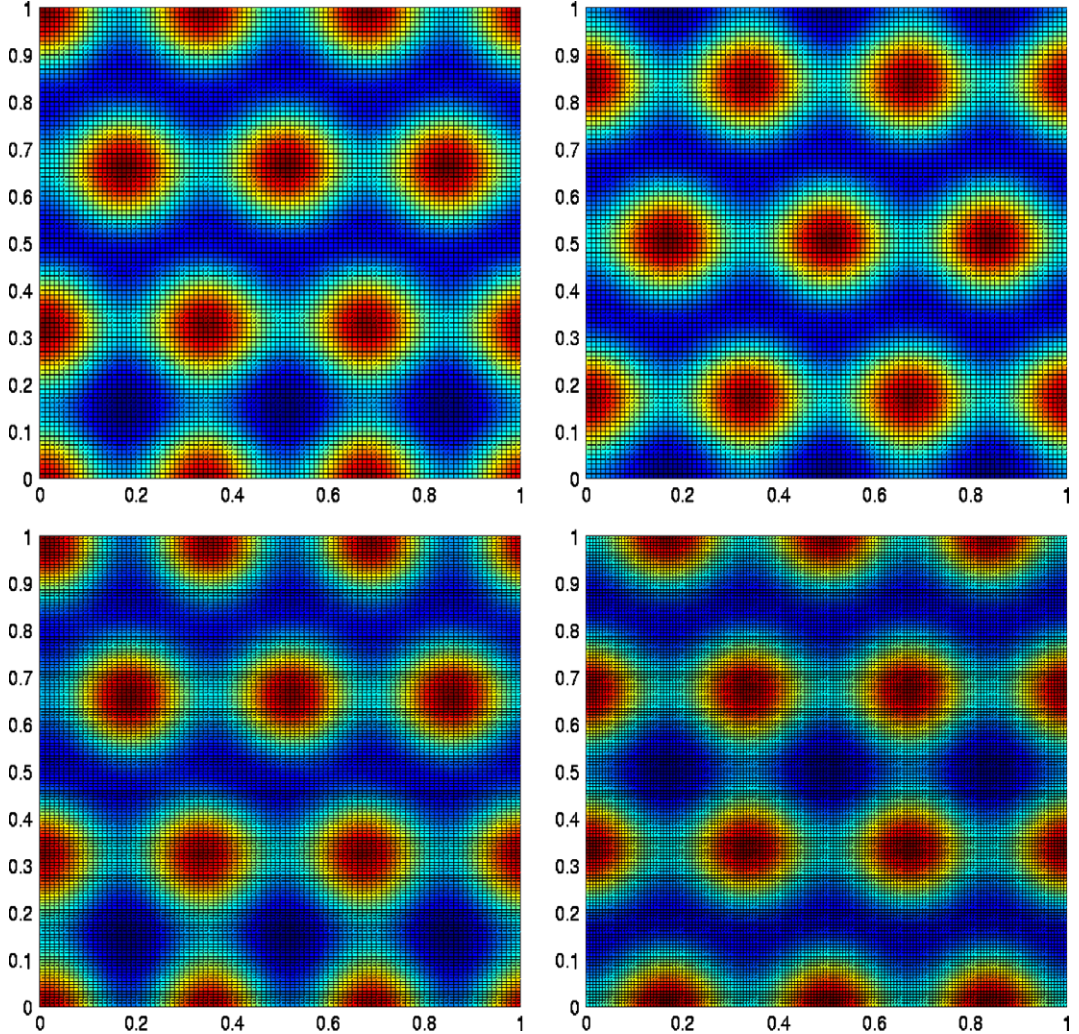


Fig. 4. Numerical solutions to the model equations computed by using the ADI method with periodic boundary conditions for different mesh sizes. Row 1: $\Delta x = \Delta y = \frac{1}{100}$. Row 2: $\Delta x = \frac{1}{150}$, $\Delta y = \frac{1}{100}$. Solutions on the left column are transient computed at time $t = 1.9$. These converge either to the top- or bottom-right steady state solution (computed at time $t = 2.0$) depending on the mesh as illustrated in Fig. 3. Folding the square domains (those on the right) into cylinders gives rise to identical patterns. Numerical and parameter values as in Fig. 3.

Fig. 5 shows computational results obtained when solving the model equations using the ADI scheme with regular mesh given by $\Delta x = \Delta y = \frac{1}{100}$ and $\Delta t = 10^{-2}$. We observe the splitting of a single spot into four spots, and then sixteen spots and so on as the domain doubles, quadruples, etc. in size. The sequence generated is 1, 4, 16, ... which translates to even powers of two, i.e. $2^0, 2^2, 2^4, \dots$. This same sequence was generated by Crampin [10] for identical model and numerical parameter values. The observation then was that the symmetrical phenomenon of this sequence is due to the square domain and the isotropic growth.

Let us solve the original model equations with identical parameter values but this time using the MGFEM-2SBDF scheme on an unstructured mesh. The unit square domain is allowed to deform uniformly and isotropically as illustrated in Fig. 6. Clearly the sequence differs completely from that shown in Fig. 5. A spot re-orientates into an oblique *peanut-like* stripe pattern which further splits diagonally into two spots. These further split diagonally into four spots and then eight and so on as the domain grows in size. The sequence generated is 1, 2, 4, 8, 16, ... which translates to simply powers of two: $2^0, 2^1, 2^2, 2^3, \dots$. Clearly, the selection process here is different from that obtained using the ADI method using a regular square mesh. We have used identical model parameter and numerical values in both numerical schemes and yet the selection process is different for each

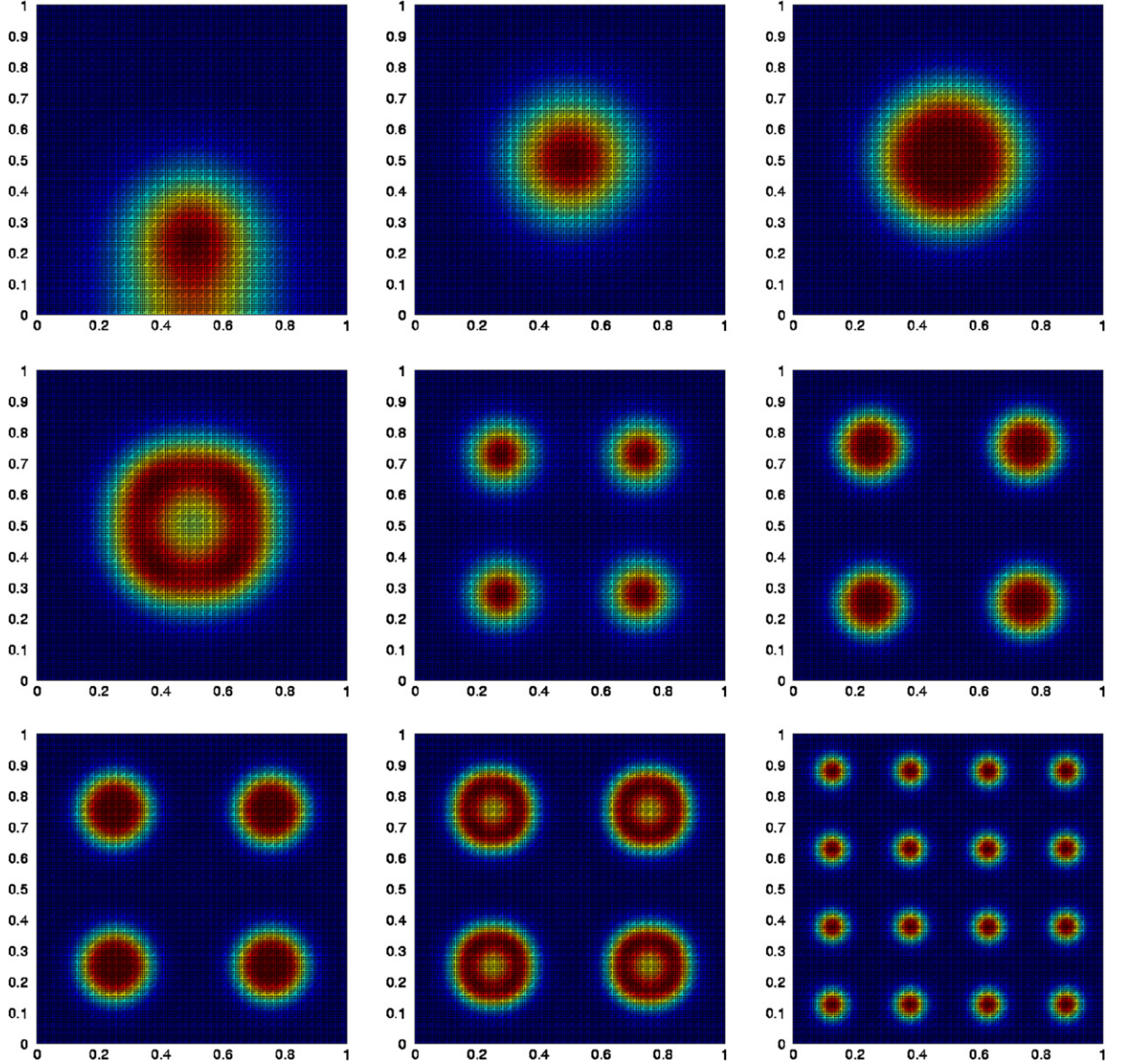


Fig. 5. The ADI transient patterns generated by the Schnakenberg model as the unit square is grown along the diagonal line $x = y$ at constant speed in the positive direction with growth rate $r = 0.002$ shown at times $t = 102, 170, 340, 408, 442, 646, 680, 748$ and 850 , respectively. The parameter values in the numerical computations are $a = 0.1$, $b = 0.9$, $d = 0.01$, $\gamma = 1.0$ and $\Delta t = 10^{-2}$. A uniform square mesh is used with $\Delta x = \Delta y = \frac{1}{100}$. Observe the spot splitting into four, sixteen and so on as the domain grows to approximately four times its original size.

scheme. A uniform square mesh structure was used in the ADI scheme as opposed to an unstructured triangular mesh for the MGFEM-2SBDF scheme. Qualitatively similar results are obtained for the MGFEM-2SBDF scheme if a regular mesh structure is used or if a regular or irregular mesh is further refined (results not shown). The crucial question is why two different numerical methods produce different results for identical numerical and model parameter values?

Instead of using uniform square mesh elements for the ADI scheme, let the mesh be rectangular defined by $\Delta x = \frac{1}{200}$ and $\Delta y = \frac{1}{100}$. Instead of square elements we have rectangles elongated along the y -axis. The parameter values remain unchanged. The results of our simulations are shown in Fig. 7. By changing the mesh from

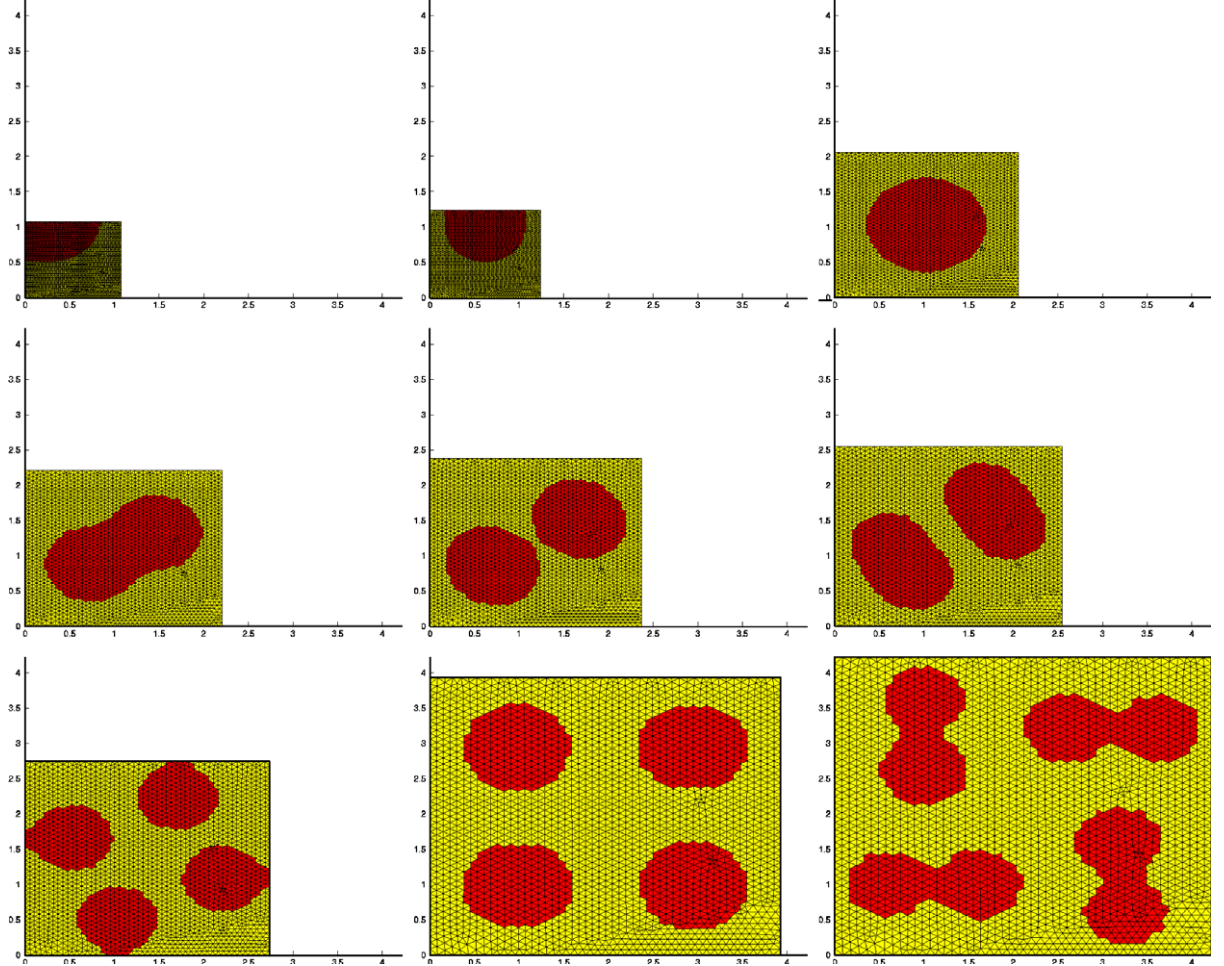


Fig. 6. The MGFEM-2SBDF transient patterns generated by the Schnakenberg model as the unit square is grown along the diagonal line $x = y$ at constant speed in the positive direction with growth rate $r = 0.002$ shown at times $t = 102, 170, 340, 408, 442, 646, 680, 748$ and 850 , respectively. The parameter values in the numerical computations are $a = 0.1$, $b = 0.9$, $d = 0.01$, $\gamma = 1.0$ and $\Delta t = 10^{-2}$. An unstructured triangular mesh is used in the numerical computations. The spot splits into two, four, eight and so on as the domain grows. Observe that the MGFEM-2SBDF scheme solves the model equations on a non-transformed continuously deforming unit square domain.

square elements to rectangular elements we obtain completely different results. The transient solutions evolve from a single spot that splits into two and these further split into four etc. The splitting process is still very regular, the splitting sequence translates to powers of two, in agreement with the sequence obtained from the MGFEM-2SBDF method. All we have changed is the structure of the mesh. The growing domain is still square at all times.

We investigate the underlying process that accounts for the different transient solutions observed for different mesh structures for the ADI method. Let us consider the growth function in terms of mesh grid points, i.e. we can write

$$x(t) = X(0)e^{rt}, \quad \text{and} \quad y(t) = Y(0)e^{rt}, \quad t > 0,$$

where $(X(0), Y(0)) \in [0, 1] \times [0, 1]$ represents the initial fixed (x, y) domain. We can therefore express the velocity of each arbitrary point $(x_i(t), y_j(t))$ as follows:

$$\frac{dx_i}{dt} = x_i(0)re^{rt} = i\Delta x re^{rt},$$

$$\frac{dy_j}{dt} = y_j(0)re^{rt} = j\Delta y re^{rt}, \quad t > 0,$$

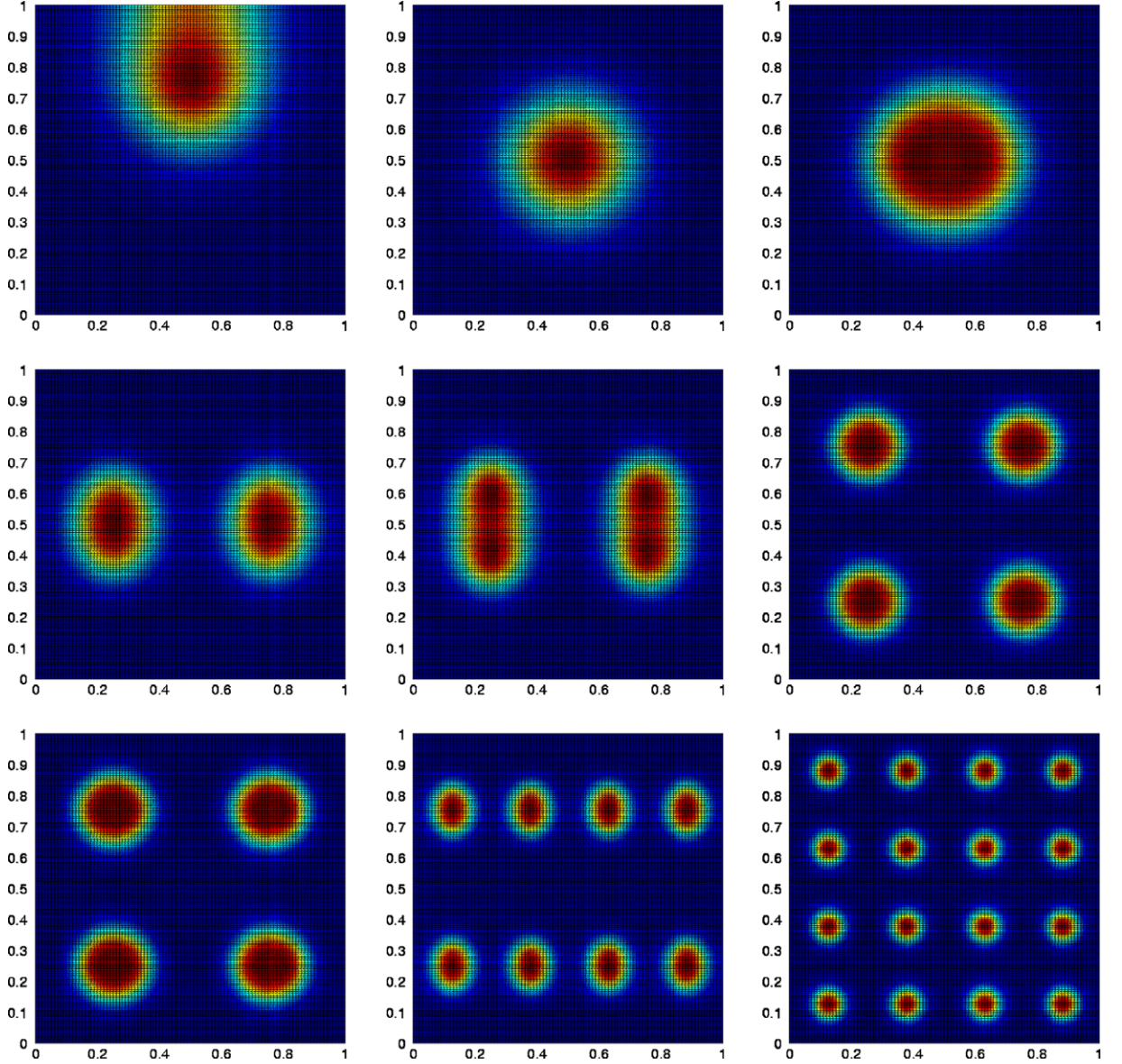


Fig. 7. The ADI transient patterns generated by the Schnakenberg model as the unit square is grown along the diagonal line $x = y$ at constant speed in the positive direction with growth rate $r = 0.002$. The snap-shots are saved at times shown in Fig. 5. The parameter values in the numerical computations are $a = 0.1$, $b = 0.9$, $d = 0.01$, $\gamma = 1.0$ and $\Delta t = 10^{-2}$. Computations are carried out on a uniform rectangular mesh given by $\Delta x = \frac{1}{200}$, and $\Delta y = \frac{1}{100}$. A single spot splits into two, four, eight and so on as the domain grows. Results are shown at times $t = 102, 170, 340, 408, 442, 646, 680, 748$ and 850 , respectively.

where each $(x_i(0), y_j(0)) \in [0, 1] \times [0, 1]$ is the initial grid point at time $t = 0$ (fixed grid points). Here we have assumed in the case of the ADI formulation that

$$x_i(0) = i\Delta x, \quad y_j(0) = j\Delta y, \quad i = 0, 1, \dots, Nx, \quad j = 0, 1, \dots, Ny,$$

where Nx and Ny are the number of grid points along the x - and y -axis respectively. The above discretization clearly shows that if the mesh is coarse, the grid points move much faster than if the mesh is refined. Although the mesh points move at different speeds depending on $x_i(t)$ and $y_j(t)$, changes in these quantities result in changes of the initial physical location of the mesh points. The ADI formulation is dependent intrinsically

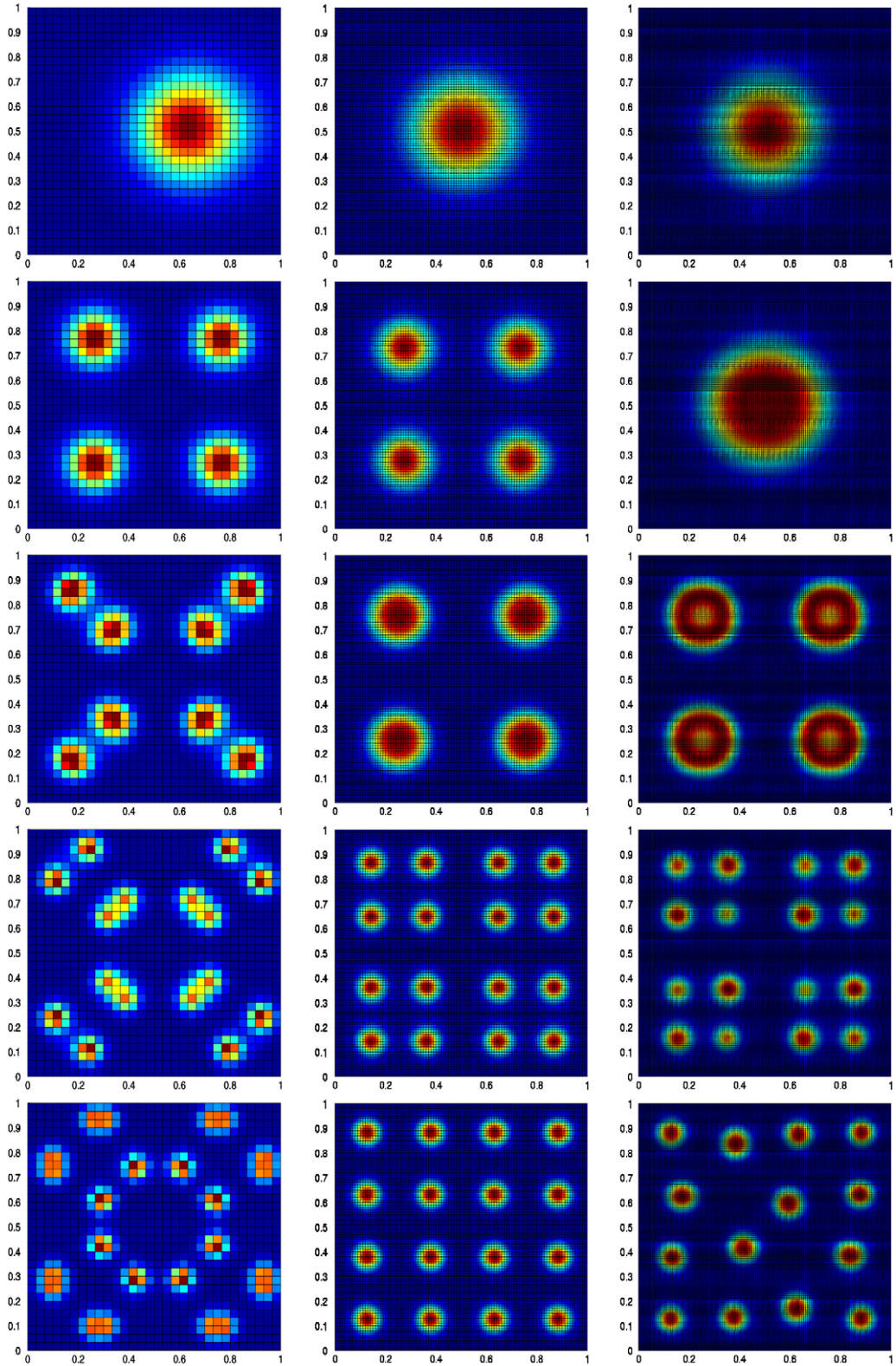


Fig. 8. A uniform square mesh refinement for the ADI scheme: Column 1: $\Delta x = \Delta y = \frac{1}{30}$, $\Delta t = \frac{1}{900}$; Column 2: $\Delta x = \Delta y = \frac{1}{100}$, $\Delta t = 10^{-2}$; and Column 3: $\Delta x = \Delta y = \frac{1}{500}$, $\Delta t = 10^{-2}$. Parameter values and the growth rate remain unchanged from those used in Fig. 5.

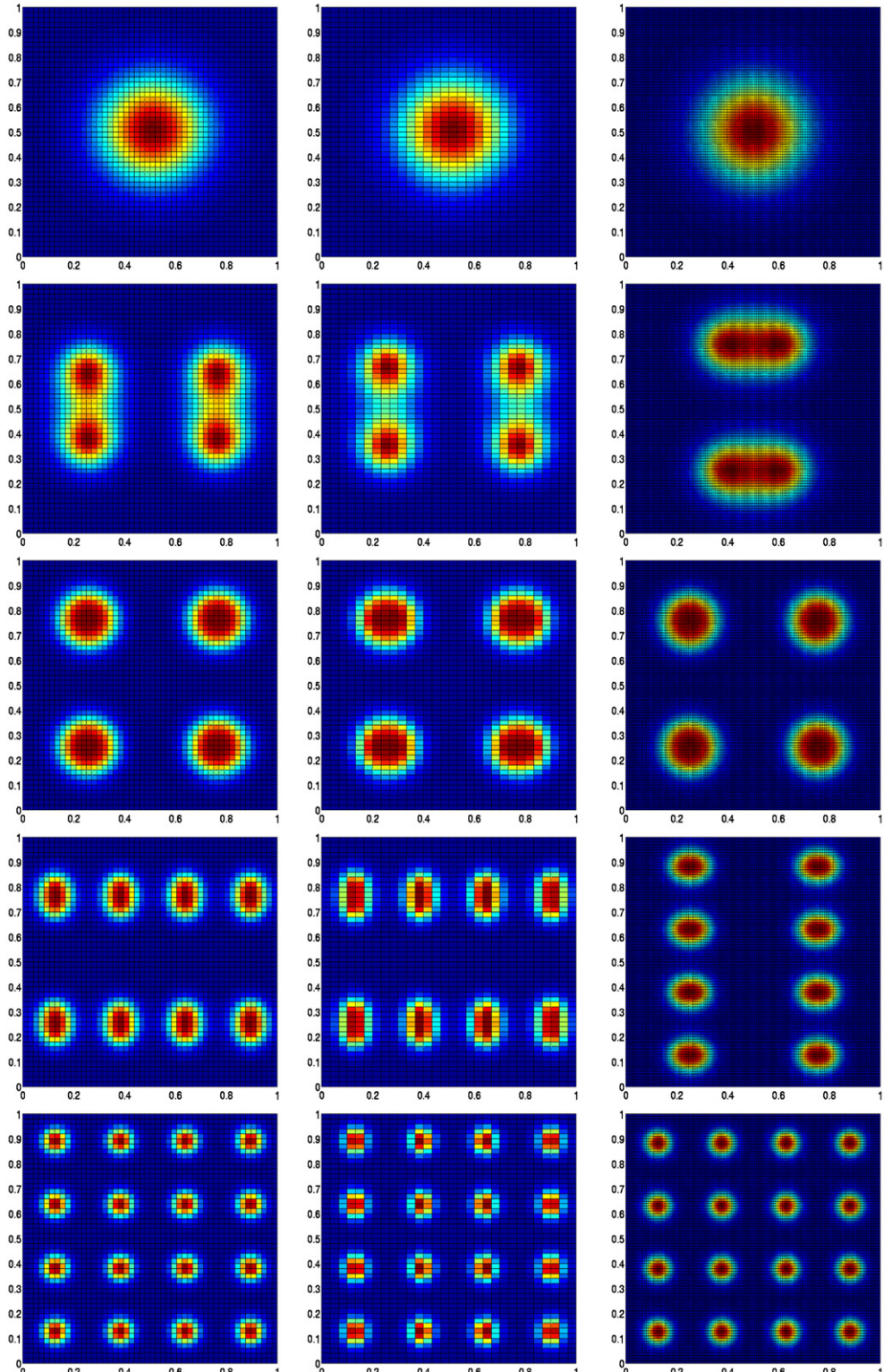


Fig. 9. A uniform rectangular mesh refinement for the ADI scheme: Column 1: $\Delta x = \frac{1}{50}$, $\Delta y = \frac{1}{49}$, $\Delta t = 10^{-2}$; Column 2: $\Delta x = \frac{1}{50}$, $\Delta y = \frac{1}{30}$, $\Delta t = 10^{-2}$; and Column 3: $\Delta x = \frac{1}{100}$, $\Delta y = \frac{1}{150}$, $\Delta t = 10^{-2}$. Parameter values and the growth rate remain unchanged from those used in Fig. 5.

on the mesh sizes Δx and Δy . The grid-point velocity on a coarse mesh is different from the grid-point velocity on a finer mesh and therefore the resolution of the computational domain influences the bifurcation process on continuously deforming domains. This observation is clearly illustrated in numerical simulations whose results are shown in Fig. 8 whereby we solve the model equations using the ADI method with successive mesh refinements. The results should be read column-wise with column 1 representing results with mesh-size $\Delta x = \Delta y = \frac{1}{30}$ shown at times $t = 102, 442, 714, 782$ and 850 . Column 2: $\Delta x = \Delta y = \frac{1}{100}$ and results are shown at times $t = 170, 442, 646, 782$ and 850 . Column 3: $\Delta x = \Delta y = \frac{1}{500}$ with results shown at times $t = 170, 340, 748, 782$, and 850 . The different times are chosen specifically to illustrate the different dynamics taking place for different grid-point velocities. The model parameter values remain unchanged with growth rate $r = 0.002$. It can be observed from the first column that a single spot splits into 4, and then 8 and 16 etc. on a coarse uniform square mesh $\Delta x = \Delta y = \frac{1}{30}$. The sequence generated is $1, 4, 8, 16, \dots$. This sequence differs from that illustrated in column 2. Here the sequence observed is $1, 4, 16, \dots$. Simply by refining the uniform square mesh to $\Delta x = \Delta y = \frac{1}{100}$, we observe different pattern sequences. Column 3 shows a very surprising result when the uniform square mesh is further refined to $\Delta x = \Delta y = \frac{1}{500}$. Although initially the splitting sequence follows that of Column 2, the pattern at time 850 is not that of 16 spots but 14 spots. This is due to the slow movement of the grid points. Numerical results on the static domain gives rise to either a 12, 13, 14 or 15 spot pattern depending on how close the initial conditions are to the selected pattern. We have carried out various numerical computations with further uniform square mesh refinement such as $\Delta x = \Delta y = \frac{1}{600}, \frac{1}{700}$ or $\frac{1}{1000}$, for example, and we have obtained similar results. So far, we carried out simulations on uniform square mesh with refinement. What if the mesh is not square?

A remarkable result is that if we perturb slightly the mesh structure, say for example, $\Delta x = \frac{1}{30}$ and $\Delta y = \frac{1}{49}$ or $\Delta x = \frac{1}{500}$ and $\Delta y = \frac{1}{499}$ we obtain the sequence $1, 2, 4, 8, 16, \dots$ as illustrated in Fig. 9. Here, a rectangular mesh structure is used. The snap-shots are shown at times $t = 170, 442, 646, 748$ and 850 for columns 1, 2 and 3 respectively. Observe that the sequences: $1, 4, 8, 16, \dots$ and $1, 4, 16, \dots$ are sub-sequences of the sequence $1, 2, 4, 8, 16, \dots$. It turns out that a uniform rectangular mesh stabilises the sequence $1, 2, 4, 8, 16, \dots$ and not the sub-sequences. Therefore the two sub-sequences are highly unstable to small or large perturbations in the mesh structure. By choosing $\Delta x \neq \Delta y$ we always obtain the sequence $1, 2, 4, 8, 16, \dots$. In Fig. 9 we illustrate results for various mesh sizes. Clearly for the ADI scheme, a square mesh stabilises the selection of different patterns depending on whether the mesh is coarse or refined and the grid-point velocity and therefore the resolution of the computational continuously deforming domain plays a crucial role in the bifurcation process. By slightly changing the structure of the mesh from square to rectangles, the sequence of simple powers of two is obtained always. These observations arise purely from a computational point of view, and more detailed study is warranted into the bifurcation theory on continuously deforming domains. One of the aims of this paper is to illustrate the need for such theory in order to understand the selection process of the transient patterns on continuously deforming domains. It must be observed that the $1, 2, 4, 8, 16, \dots$ sequence can be obtained also by taking for example the growth rate in the y -direction to be twice the growth rate in the x -direction. For example, taking $r_x = 0.001$ and $r_y = 0.002$ with $\Delta x = \Delta y$ yields the same sequence. Although we are taking a square mesh structure, the growth rate overrides the influence of the mesh structure in the selection process. The splitting process for this scenario will favour the x -axis rather than the y -axis and vice-versa if the growth rates are switched around.

In certain cases, we have shown that numerical solutions on growing domains are independent of the initial conditions (these are prescribed as random small perturbations around the uniform steady state). This is due to domain growth which enhances robust selection of the transient patterns (Crankin et al. [11], Madzvamuse et al. [22]). The ADI and MGFEM-2SBDF yield the observed bifurcation sequences independent of the initial conditions.

6. Conclusions and discussion

When solving reaction-diffusion equations on continuously deforming domains, domain growth and grid-point velocity are additional parameters that greatly influence the selection of transient patterns. In applying numerical methods to partial differential equations it is important to be aware of the role of mesh structure (grid-point velocity) and its influence on numerical solutions for reaction-diffusion systems on continuously

growing domains. In particular, the finite difference scheme can yield different solutions for different types of mesh structure. On fixed domains, it seems that the rectangular finite difference scheme (split-step) imposes implicitly in its construction (using regular equal mesh) symmetrical solutions on regular domains. This same phenomenon has been observed in simulations by Kassam and Trefethen [15,16]. By solving reaction-diffusion equations using exponential time difference (a spectral method) fourth-order Runge–Kutta method non-symmetric solutions were obtained on regular domains in contrast to symmetrical regular solutions obtained from the finite difference scheme.

Here we have presented solutions obtained using the ADI and MGFEM-2SBDF methods. The nodal-grid-point velocity for the MGFEM-2SBDF scheme does not influence the bifurcation process of the transient solutions on continuously growing domains due to the nature of its formulation which is independent of the mesh structure. One can think of the nodal-grid-points of the unstructured mesh for the MGFEM-2SBDF method as randomly placed points on the planar domain. This is not the case with the ADI method. For this method we have shown, through simulations, how incorporating domain growth creates an added parameter – the grid-point velocity – which in turn stabilises certain symmetric patterns when a regular uniform square mesh is used. The grid-point velocity seems to play a pivotal role in influencing the bifurcation process in pattern selection depending on how slow (refined mesh) or fast (coarse mesh) the grid points move. We have been able to compute the sequences 1, 4, 8, 16,... and 1, 4, 16,... using a uniform square mesh structure. These sequences are obtained by simply changing the uniform square mesh from a coarse to a refined mesh respectively. There is an underlying bifurcation process related to the grid-point velocity depending on whether it is a coarse or a refined mesh. However, by changing the structure of the uniform square mesh to a uniform rectangular mesh, the above two sequences become unstable and only the sequence 1, 2, 4, 16,... is obtained. This is independent of whether the mesh is coarse or refined. Refining the square structure mesh implies a slower grid-point movement thereby weakening the role of grid-point velocity in the bifurcation selection process. In this case the bifurcation process occurs much later than on a coarse mesh. This can be seen in simulations shown in Fig. 8. Observe that the sequences illustrated here for each column are recorded at different times because of the nature of the mesh structure. The four spot pattern appears much earlier on a coarse mesh than on a refined mesh, for example.

The results shown in this paper were also obtained by taking a refined timestep Δt to the orders of 10^{-4} and therefore our results are robust to timestep refinement. However, on a continuously deforming domain, taking a time-step less than 10^{-4} implies that the computations are prohibitively expensive due to the fact that this is a growing domain problem (Madzvamuse, [19]).

Figs. 5–9 show transient solutions on a continuously deforming unit square domain. We have carried out numerical simulations to compute the spatially inhomogeneous steady state solutions on the final fixed square domain using the ADI and MGFEM-2SBDF methods starting with random initial conditions. Both schemes converge to either 12, 13, 14, 15 or 16 spots (results not shown). The finite element results are independent of the structure of the mesh and the choice really depends on how close the initial conditions are to the selected pattern. The “peanut” patterns observed in Fig. 6 re-organise into one of the 12, 13, 14, 15 or 16 spot patterns once the final domain has stopped growing and the simulation is allowed to converge to a steady state (results not shown). For the ADI method the solution converged to does not only depend on the basis of attraction given by the initial conditions but also on the structure of the mesh. The selection of the regularly organised spot patterns 1, 4, 8, 16,... or 1, 4, 16,... are independent of the initial conditions, domain growth robustly enhances the selection process (except for the ADI scheme where the mesh structure influences the transition process). On a fixed domain to compute 16 spots one needs to precisely choose initial conditions which are very close to the 16-spot steady state. In this sense, the work here extends that of Crampin et al. [9] who showed that on one-dimensional domains, growth can select and stabilise patterns through the process of mode-doubling, but that this can be disrupted by noise, which may be due to the numerical scheme used (Bar-rass, et al. [2]).

From the numerical experiments presented in this paper, it is clear that a better understanding of the bifurcation theory on continuously deforming domains is required. This is not a trivial issue, to our knowledge no such analysis or theory has been developed on continuously deforming domains. Golubitsky and Comanici have illustrated patterns on growing square domains via mode interactions (private manuscript) for linearised systems. Our case is different, these are highly nonlinear systems. Equally important is a more detailed numer-

ical analysis on artificial diffusion which depends on mesh structure and domain growth. Work in this direction is underway with studies carried out by Mckenzie and Mekwi [18]. Here they investigate the stability and convergence of time integration schemes for the solution of a semi-discretisation of a single parabolic problem in one dimension using a moving mesh. Their results show that the backward Euler scheme is unconditionally stable in a mesh dependent L_2 norm. Our model equations are much more complicated than a simple heat equation, however the theoretical framework developed in their paper gives us a platform to start a detailed numerical analysis on artificial diffusion for nonlinear systems. This is the subject of our current studies.

Acknowledgments

AM would like to acknowledge financial support from the College of Science and Mathematics (COSAM), Auburn University. We thank Drs. Andrew J. Wathen (Oxford University, UK), Angelique Stephanou (TIMC lab, Grenoble, France) and Asheber Abebe (Auburn University) for useful discussion and comments.

References

- [1] M.J. Baines, Moving Finite Elements, Monographs on Numerical Analysis, Clarendon Press, Oxford, 1994.
- [2] I. Barrass, P.K. Maini, E.J. Crampin, Mode transitions in a model reaction-diffusion system driven by domain growth and noise, *Bull. Math. Biol.* 68 (2006) 981–995.
- [3] R.A. Barrio, C. Varea, J.L. Aragón, P.K. Maini, A two-dimensional numerical study of spatial pattern formation in interacting systems, *Bull. Math. Biol.* 61 (1999) 483–505.
- [4] R.A. Barrio, P.K. Maini, J.L. Aragón, M. Torres, Size-dependent symmetry breaking in models for morphogenesis, *Physica D* 2920 (2002) 1–12.
- [5] J.P. Boyd, Chebyshev and Fourier Spectral Methods, Springer-Verlag, 1989.
- [6] W. Cao, W. Huang, R.D. Russell, An r-adaptive finite element method based upon moving mesh PDEs, *J. Comput. Phys.* 149 (1999) 221–244.
- [7] M. Chaplain, A.J. Ganesh, I.G. Graham, Spatio-temporal pattern formation on spherical surfaces: Numerical simulation and application to solid tumor growth, *J. Math. Biol.* 42 (2001) 387–423.
- [8] S.M. Cox, P.C. Matthews, Exponential time differencing for stiff systems, *J. Comp. Phys.* 176 (1988) 430–455.
- [9] E.J. Crampin, E.A. Gaffney, P.K. Maini, Reaction and diffusion on growing domains: Scenarios for robust pattern formation *Bull. Math. Biol.* 61 (1999) 1093–1120.
- [10] E.J. Crampin, Reaction-diffusion patterns in growing domains, D Phil. thesis, University of Oxford, 2000.
- [11] E.J. Crampin, W.W. Hackborn, P.K. Maini, Pattern formation in reaction-diffusion models with nonuniform domain growth, *Bull. Math. Biol.* 64 (2002) 746–769.
- [12] V. Cristini, J. Blawzdziewicz, M. Lowengrub, An adaptive mesh algorithm for evolving surfaces: simulations of drop breakup and coalescence, *J. Comp. Phys.* 168 (2001) 445–486.
- [13] A. Geirer, H. Meinhardt, A theory of biological pattern formation, *Kybernetik* 12 (1972) 30–39.
- [14] C. Johnson, Numerical Solution of Partial Differential Equations by the Finite Element Method, Cambridge University Press, 1987.
- [15] A. Kassam, L.N. Trefethen, Fourth-order time stepping for stiff PDEs, *SIAM J. Sci. Comp.* 26 (4) (2005) 1214–1233.
- [16] A. Kassam, L.N. Trefethen, Solving reaction-diffusion equations 10 times faster, Oxford University, Numerical Analysis Group Research Report No. 16, 2003.
- [17] S. Kondo, R. Asai, A reaction-diffusion wave on the skin of the marine anglefish, *Pomacanthus*, *Nature* 376 (1995) 765–768.
- [18] J.A. Mackenzie, W.R. Mekwi, An analysis of stability and convergence of a finite difference discretization of a model parabolic PDE in 1-D using a moving mesh, *IMA J. Numer. Anal.* (2006).
- [19] A. Madzvamuse, Time-stepping schemes for moving grid finite elements applied to reaction-diffusion systems on fixed and growing domains, *J. Comp. Phys.* 24 (1) (2005) 239–263.
- [20] A. Madzvamuse, A.J. Wathen, P.K. Maini, A moving grid finite element method for the simulation of pattern generation by Turing models on growing domains, *J. Sci. Comp.* 24 (2) (2005) 247–262.
- [21] A. Madzvamuse, T. Sekimura, R.D.K. Thomas, A.J. Wathen, P.K. Maini, A moving grid finite element method for the study of spatial pattern formation in Biological problems, in: T. Sekimura, S. Noji, N. Nueno, P.K. Maini (Eds.), *Morphogenesis and Pattern Formation in Biological Systems – Experiments and Models*, Springer-Verlag, Tokyo, 2003, pp. 59–65.
- [22] A. Madzvamuse, P.K. Maini, A.J. Wathen, A moving grid finite element method applied to a model biological pattern generator, *J. Comp. Phys.* 190 (2003) 478–500.
- [23] A. Madzvamuse, R.D.K. Thomas, P.K. Maini, A.J. Wathen, A numerical approach to the study of spatial pattern formation in the ligaments of arcoïd bivalves, *Bull. Math. Biol.* 64 (2002) 501–530.
- [24] A. Madzvamuse, T. Sekimura, A.J. Wathen, P.K. Maini, A predictive model for colour pattern formation in the butterfly wing of *Papilio dardanus*, *Hiroshima Math J* 32 (2002) 325–336.
- [25] A. Madzvamuse, A numerical approach to the study of spatial pattern formation, D Phil thesis, University of Oxford, 2000.
- [26] H. Meinhardt, *Models of Biological Pattern Formation*, Academic Press, New York, 1982.

- [27] H. Meinhardt, The Algorithmic Beauty of Sea Shells, Springer-Verlag, Heidelberg, New York, 1995.
- [28] K.W. Morton, Numerical Solution of Convection-Diffusion Problems, Chapman and Hall, 1996.
- [29] K.W. Morton, D.F. Mayers, Numerical Solution of Partial Differential Equations, Cambridge University Press, 1994.
- [30] J.D. Müller, P.L. Roe, H. Deconinck, A frontal approach for internal node generation for Delaunay triangulation, Int. J. Numer. Meth. Fluids. 17 (3) (1993) 241–256.
- [31] J.D. Murray, A prepatter formation mechanism for animal coat markings, J. Theor. Biol. 88 (1981) 161–199.
- [32] J.D. Murray, Mathematical Biology I and II, 3rd edn., Springer-Verlag, Berlin, 2002.
- [33] F.H. Nijhout, P.K. Maini, A. Madzvamuse, A.J. Wathen, T. Sekimura, Pigmentation pattern formation in butterflies – experiments and models, Comptes Rendus Biologies 328 (8) (2003) 711–727.
- [34] K.J. Painter, H.G. Othmer, P.K. Maini, Stripe formation in juvenile Pomacanthus explained by a generalized Turing mechanism with chemotaxis, Proc. Natl. Acad. Sci. 96 (1999) 5549–5554.
- [35] D.W. Peaceman, H.H. Rachford Jr., The numerical solution of parabolic and elliptic differential equations, J. Soc. Ind. Appl. Math. 3 (1) (1955) 28–41.
- [36] R.G. Plaza, F. Sánchez-Garduño, P. Padilla, R.A. Barrio, P.K. Maini, The effect of growth and curvature on pattern formation, J. Dynam. Diff. Eqs. 16 (4) (2004) 1093–1121.
- [37] T.N. Reddy, An Introduction to the Finite Element Method, McGraw-Hill, 1984.
- [38] S.J. Ruuth, Implicit-explicit methods for reaction-diffusion problems in pattern formation, J. Math. Biol. 34 (2) (1995) 148–176.
- [39] Y. Saad, Iterative Methods for Sparse Linear Systems, PWS Publishing Co, 1996.
- [40] T. Sekimura, A. Madzvamuse, A.J. Wathen, P.K. Maini, A model for colour pattern formation in the butterfly wing of *Papilio dardanus*, Proc. Roy. Soc. London. Series B 26 (2000) 851–859.
- [41] J. Schnakenberg, Simple chemical reaction systems with limit cycle behaviour, J. Theor. Biol. 81 (1979) 389–400.
- [42] E. Tadmor, The exponential accuracy of Fourier and Chebyshev differencing methods, SIAM J. Numer. Anal. 23 (1) (1986) 1–10.
- [43] A. Turing, The chemical basis of morphogenesis, Phil. Trans. R. Soc. Lond. B 237 (1952) 37–72.
- [44] X. Zheng, S.M. Wise, V. Cristini, Nonlinear simulation of tumor necrosis, neo-vascularization and tissue invasion via an adaptive finite-element/level-set method, Bul. Math. Biol. 67 (2004) 211–259.